

Identification of chronic obstructive pulmonary disease using graph convolutional network in electronic nose

Dava Aulia¹, Riyanarto Sarno¹, Shintami Chusnul Hidayati¹, Alfian Nur Rosyid^{2,3}, Muhammad Rivai⁴

¹Department of Informatics, Faculty of Intelligent Electrical and Informatics Technology, Institut Teknologi Sepuluh Nopember, Surabaya, Indonesia

²Universitas Airlangga Hospital, Faculty of Medicine, Universitas Airlangga, Surabaya, Indonesia

³Department of Pulmonology and Respiratory Medicine, Faculty of Medicine, Universitas Airlangga, Surabaya, Indonesia

⁴Department of Electrical Engineering, Faculty of Intelligent Electrical and Informatics Technology, Institut Teknologi Sepuluh Nopember, Surabaya, Indonesia

Article Info

Article history:

Received Dec 29, 2023

Revised Jan 17, 2024

Accepted Jan 24, 2024

Keywords:

COPD

Diseases

Electronic nose

Exhaled breath

Graph convolutional network

ABSTRACT

Chronic obstructive pulmonary disease (COPD) is a progressive lung dysfunction that can be triggered by exposure to chemicals. This disease can be identified with spirometry, but the patient feels uncomfortable, affecting the diagnosis results. Other disease markers are being investigated, including exhaled breath. This method can be applied easily, is non-invasive, has minimal side effects, and provides accurate results. This study applies the electronic nose method to distinguish healthy people and COPD suspects using exhaled breath samples. Twenty semiconductor gas sensors combined with machine learning algorithms were employed as an electronic nose system. Experimental results show that the frequency feature of the sensor responses used by the principal component analysis (PCA) method combined with graph convolutional network (GCN) can provide the highest accuracy value of 97.5% in distinguishing between healthy and COPD subjects. This method can improve the detection performance of electronic nose systems, which can help diagnose COPD.

This is an open access article under the [CC BY-SA](https://creativecommons.org/licenses/by-sa/4.0/) license.



Corresponding Author:

Riyanarto Sarno

Department of Informatics, Faculty of Intelligent Electrical and Informatics Technology

Institut Teknologi Sepuluh Nopember

Keputih, Sukolilo, Surabaya, East Java 6011, Indonesia

Email: riyanarto@if.its.ac.id

1. INTRODUCTION

Chronic obstructive pulmonary disease (COPD) can be triggered chiefly by chemical exposure to cigarette smoke [1]. This impulse permanently wounds the lung due to inflammation indicated by airflow restriction. Therefore, COPD sufferers often have difficulty breathing [2]. COPD is not a contagious disorder. This disease occurs in men over 40 years old and is influenced by long-term vulnerability substances [3]. COPD is similar to asthma despite progressive and can worsen [1], [2]. In 2019, COPD has affected 3.23 million people [4]. For this reason, the issue needs immediate awareness.

Spirometry can identify COPD, which is still impractical and uncomfortable, influencing the results. Other disease markers are being investigated, including exhaled breath [5]. This non-invasive method provides more comfort to the patient and accurate results [6]. Exhaled breath contains chemicals that can be used for analytical purposes, especially volatile organic compounds [7]. Gas chromatography can assess these compounds but is still limited and costly. An electronic nose comprises chemical gas sensors, offering an odor-

detection means inspired by the human nose function. This approach is an alternative way to detect human body abnormalities [8]–[11].

The electronic nose reliability can be defined by its effectiveness in extracting relevant features from the sensor signal response. An electronic nose has organized healthy and asthmatic subjects with the support vector machine (SVM), supplying an accuracy of 89.5% [12]. Data is extracted in a time range between 30-49 seconds to obtain an average value. Another study categorizes different lung diseases, with 50-second sampling and kernel principal component analysis combined with extreme gradient boosting (KPCA-XGBoost) as feature extraction and classifier strategies yielding 89.84% for COPD [9]. Tuberculosis was also examined using an artificial neural network (ANN) along with standardization with an accuracy of 94.87% [8]. However, these studies only use standard features in the time domain. More information on transient signals is needed to improve classification performance.

The transient response before reaching a steady state can be considered as a characteristic for classification purposes [13]. Fast fourier transform (FFT) is a signal preprocessing technique for efficiently analyzing frequency elements in discrete signals [14]. With its computational efficiency capabilities, FFT can process faster than discrete Fourier transform (DFT), simplifying the DFT time complexity to minimize computational costs [15]. FFT can be applied in transient signal events, such as in electronic noses [16].

Graph convolutional network (GCN) employs convolution operations on graph structures. One is spatial graph convolution, which uses adjacency matrix computation, focusing on the neighboring nodes' affinity and justifying the nodes' representation based on information from their neighbors [17]. This approach captures local dependencies and relationships within the data, effectively handles large-dimensional graphs, controls irregular data structures, and apprehends complex relationships [18]. Entities linked by edge demonstrate the main attribute of GCN; they are non-Euclidean and primary learning sources for GCN. The graph representation is the input of the GCN and can be represented as an adjacency matrix. This matrix can be obtained by calculating the relationship between attributes, one of which is using correlation techniques [19]. Another study gave sufficient results using this approach with an electronic nose [19].

The main contribution of this study is to develop a method to differentiate healthy people and COPD suspects based on exhaled breath samples using an electronic nose and the GCN algorithm. The adjacency matrix is calculated with the Pearson correlation coefficient (PCC) to construct the GCN feature map. Frequency elements of sensor response and principal component analysis (PCA) data preprocessing are involved in increasing the distinguishing accuracy.

The novelty of this study includes implementing a GCN method with frequency feature to achieve a reliable electronic nose indicating healthy and COPD subjects. This article is systematized as follows. The research background is described in section 1. Section 2 presents the materials and methods of the experiments. In section 3 explains the experimental results and their analysis. In section 4 outlines influential outcomes and forthcoming studies.

2. MATERIALS AND METHODS

2.1. Subjects and research design

Exhaled breath data was collected at Airlangga University General Hospital, East Java, Surabaya, Indonesia. The subjects included 30 healthy people and 40 COPD suspects, as confirmed by pulmonologists, comprised of men aged between 50 and 70 years without acute or chronic conditions and healthy non-smokers. Pulmonary function tests diagnosed COPD with a CONTEC SP70B digital spirometer, where a ratio between forced expiratory volume in the first second (FEV1) and forced vital capacity (FVC) below 70% is verified as a suspect. Experts have examined further through clinical analysis, including COPD assessment test (CAT) and pulmonary medical history and assessment (PUMA).

The study design is presented in Figure 1. All participants supplied a breath sample in a 2-liter Tedlar bag. The electronic nose is a measuring device, producing different curves for each sensor response. Signal preprocessing involves the sensor signal response, including time and frequency domains as features. The sensor response is divided into four segments for the classification dataset. Random forest (RF), ANN, convolutional neural network (CNN), gated recurrent unit (GRU), and GCN are machine learning algorithms and are optimized with various architectures. The adjacency matrix describes the graph representation as GCN input determined through the PCC. The PCA is involved for comparison purposes. The models' classifier appraisal has accuracy, precision, recall, and F1 measurements.

2.2. Electronic nose

Figure 2 shows the equipment setup used in this experiment. Figure 2(a) describes the design of the electronic nose. Electronic parts are mounted on a printed circuit board (PCB), making the sensors' responses more stable [20]. Metal oxide semiconductor gas sensors are utilized for their advantages: cheapness, durability, and high sensitivity [21], [22], as depicted in Table 1. Twenty gas sensors will contribute to measuring gas content

in exhaled breath related to healthy and COPD subjects, and some sensors can detect biomarkers associated with lung disease effectively [8]–[10]. The sensor array is installed in the 150 mL chamber. Flowmeter allows for monitoring airflow speed. Meanwhile, Figure 2(b) depicts the implementation of the system.

The sampling steps are as follows. The sample in the Tedlar bag is measured for 100 seconds, followed by cleaning the sensors with dry air at the recovery stage. The sensor's analog voltage is converted to digital using the microcontroller's data converter. Data is transmitted to a computer and managed in a spreadsheet program. The dataset consists of response curves for the subsequent analysis of signal processing.

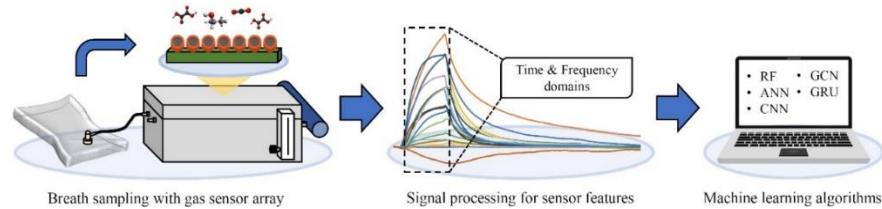


Figure 1. The proposed research diagram



Figure 2. The electronic nose setup in the investigation (a) system design and (b) implementation

Table 1. Types of gas sensors on electronic nose

Sensor	Sensitivity
MQ-2	Hydrogen, LPG, and propane
MQ-3	Benzene and alcohol
MQ-4	LPG and methane
MQ-5	Methane, LPG, and carbon monoxide
MQ-6	Butane, propane, and LPG
MQ-7	Carbon monoxide and hydrogen
MQ-8	Hydrogen
MQ-9	Methane, carbon monoxide, and LPG
MQ-131	Nitrogen dioxide, ozone, and chlorine
MQ-135	Ammonium, acetone, and toluene
MQ-136	Ammonium, hydrogen sulfide
MQ-137	Ammonia
TGS813	Isobutane, hydrogen, ethanol, and methane
TGS822	Hexane, benzene, and ethanol
TGS2600	Ethanol, hydrogen, and isobutane
TGS2602	Hydrogen sulfide, ammonia, and ethanol
TGS2610	Methane, hydrogen, isobutane, and ethanol
TGS2611	Isobutane, methane, ethanol, and hydrogen
TGS2620	Isobutane, hydrogen, and ethanol
TGS4161	Carbon dioxide

2.3. Signal processing

Two features, including time and frequency elements, are used for comparison purposes. The feature extraction procedure is as follows:

- Transient is a region of interest, starting in the 10th second until before reaching a steady state.
- The signal is divided into four parts, each 20 seconds long.
- Each signal section will provide both time and frequency elements.

The time average value of each sensor data can be represented in (1).

$$\bar{x}_s = \frac{\sum_{n=0}^{N-1} x_s^n}{N} \tag{1}$$

Where N denotes the number of samples, s describes the sensor number, and x_s^n represents the sensor response at time n for sensor s . The frequency elements can be expressed in (2).

$$X_s^k = \int_{n=0}^{N-1} x_s^n \cdot e^{-j\frac{2\pi}{N}kn} \tag{2}$$

Where e is the base of the natural logarithm, and j is the imaginary unit.

2.4. Machine learning algorithms

2.4.1. RF

The RF algorithm is often combined with the electronic nose method with satisfactory results [23], [24]. With bagging systems, RF combines multiple decision trees to build respective outputs and draw conclusions through majority voting [25]. RF criteria, including the Gini index and entropy, decide the optimal splitting nodes for forming the finest decision tree, clarified in (3) and (4).

$$Gini\ index = 1 - \sum_{j=1}^N (p_j)^2 \tag{3}$$

$$Entropy = - \sum_{j=1}^N (p_j * \log_2(p_j)) \tag{4}$$

Where N designates the number of categories and p_j means the data portion in class j . In this study, the RF parameters include criterion: Gini index and entropy, max_features: \log_2 and sqrt, max_depth: none, tress: 1-200, min_samples_split: 2-6, and min_samples_leaf: 2-4.

2.4.2. ANN

ANN is a pattern recognition technique encouraged by the human brain function, which involves three main layers: input, hidden, and output [26]. The number of nodes in the input layer follows the number of sensor features. The hidden layers comprise neurons by calculating the weighted sum through the rectified linear unit (ReLU) activation function. The output layer contains neurons that use softmax activation to represent the number of class data. ANN offers feed-forward and back-propagation processes, where the former confines decisions, and the latter revises the weights based on the error value. Table 2 reveals the ANN configuration.

Table 2. The configurable ANN and CNN layer settings

Model	Hidden layers			Model	Filters		Kernels		Neurons
	1	2	3		Conv 1	Conv 2	Conv 1	Conv 2	
ANN 1	5			CNN 1	5				5
ANN 2	30	-		CNN 2	30		2		30
ANN 3	55			CNN 3	55				55
ANN 4	5	5		CNN 4	5	-			5
ANN 5	30	5		CNN 5	30		3		30
ANN 6	30	30		CNN 6	55				55
ANN 7	55	30		CNN 7	5	5			5
ANN 8	55	55		CNN 8	30	5			30
ANN 9	5	5	5	CNN 9	30	30	2		30
ANN 10	30	5	5	CNN 10	55	30			55
ANN 11	30	30	5	CNN 11	55	55			55
ANN 12	30	30	30	CNN 12	5	5		2	5
ANN 13	55	30	30	CNN 13	30	5			30
ANN 14	55	55	30	CNN 14	30	30	3		30
ANN 15	55	55	55	CNN 15	55	30			55
				CNN 16	55	55			55

2.4.3. CNN

1D CNN is specialized for sequential data due to its mechanism involving convolutional layers called conv. This layer contains filters and kernels to extract patterns or features from the input dataset [11]. This model presents feed-forward and backpropagation approaches similar to ANN [27]. CNN has proved to better distinguish between healthy and asthmatic subjects [10]. The number of neurons in the fully connected layer is also considered to determine the level of accuracy. Table 2 characterizes the CNN architectural format, consisting of the number of convs, filters, kernels, and neurons.

2.4.4. GRU

GRU has different means than long short-term memory (LSTM), including the simpler architecture by eliminating forget gates to improve computational efficiency [28]. The update and reset gates, the primary gates of GRU, are presented to analyze the data flow within the unit, authorizing it to keep and discard data adaptively over various periods [29]. This study involves five GRU algorithms, including GRU 1, GRU 2, GRU 3, GRU 4, and GRU 5, with memory cells of 5, 30, 55, 80, and 105, respectively.

2.4.3. GCN

GCN analyzes the input graph of sensor features to provide classification results. Each sensor's time and frequency elements represent nodes; each node is only connected to its neighboring nodes with its edges. Therefore, this dataset is an undirected graph. The undirected graph is expressed in (5).

$$G = \{V, E, A\} \tag{5}$$

Where V is the vertices or nodes defining sensor features, E represents the set of edges, and A is the adjacency matrix expressing the connection among all features. PCC values replace the adjacency matrix elements between sensor features [19], represented in (6). Therefore, the adjacency matrix can be described in (7).

$$r = \frac{\sum_{i=1}^n (x_i - \bar{x})(y_i - \bar{y})}{\sqrt{\sum_{i=1}^n (x_i - \bar{x})^2 \sum_{i=1}^n (y_i - \bar{y})^2}} \tag{6}$$

$$A = \begin{bmatrix} 0 & r_{1,2} & \dots & r_{1,n} \\ r_{2,1} & 0 & \dots & r_{2,n} \\ \vdots & \vdots & \ddots & \vdots \\ r_{n,1} & r_{n,2} & \dots & 0 \end{bmatrix} \tag{7}$$

The propagation of the convolution layer is depicted in (8).

$$H^{(l+1)} = f(\hat{D}^{-\frac{1}{2}} \hat{A} \hat{D}^{-\frac{1}{2}} H^{(l)} W^{(l)}) \tag{8}$$

Where f is the activation function, $H^{(l)}$ and $W^{(l)}$ are the node feature matrix and weights at layer (i), respectively. Figure 3 and Table 3 illustrate the feature graph construction and the GCN configuration, respectively.

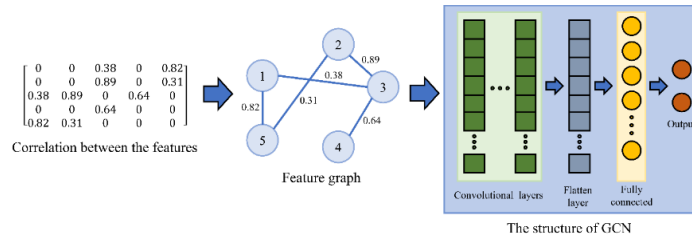


Figure 3. The feature graph construction of the GCN

Model	Convs			Fully connected
	1	2	3	
GCN 1	5			
GCN 2	30	-		
GCN 3	55			
GCN 4	5	5		
GCN 5	30	5	-	
GCN 6	30	30		
GCN 7	55	30		
GCN 8	55	55		5, 30, 55
GCN 9	5	5	5	
GCN 10	30	5	5	
GCN 11	30	30	5	
GCN 12	30	30	30	
GCN 13	55	30	30	
GCN 14	55	30	30	
GCN 15	55	55	55	

2.5. Classifier performance evaluation

The confusion matrix assesses the classifier’s performance by approximating the classified data with the actual truth through accuracy, precision, recall, and F1-score. These metrics are based on several indicators, such as true positive (TP), false positive (FP), true negative (TN), and false negative (FN). The performance evaluations can be acquired in (9) to (12).

$$Accuracy = \frac{TP+TN}{TP+FN+TN+FP} \tag{9}$$

$$Precision = \frac{TP}{TP+FP} \tag{10}$$

$$Recall = \frac{TP}{TP+FN} \tag{11}$$

$$F1 - Score = \frac{2 \times Precision \times Recall}{Precision + Recall} \tag{12}$$

2.6. PCA

PCA is a technique for dimensionality reduction, summarizing extensive datasets into simpler ones while retaining important information. PCA transforms data with a linear orthogonal transformation to form new coordinates into PCA space [30]. This transformation is achieved by selecting principal components with a high contribution to the linear combination of the original features. This study applies this technique to visualize and preprocess the sensor features.

3. EXPERIMENTAL RESULTS

3.1. Dataset preparation

All exhaled breath samples stored in the Tedlar bags were acquired by electronic nose. Figure 4 depicts the sensor response in the time domain. The response at 0 to 10 seconds is the initial cleaning or baseline determination, while the points at 11 to 100 seconds are used as sample recording data. The sensor responses for healthy and COPD subjects are shown in Figures 4(a) and 4(b), respectively. These show that each class has a distinctive curve pattern, making it manageable to analyze. Figure 5 demonstrates the feature extraction strategy. Most of these regions are transient and used as features for time and frequency extraction. As a result, four regions were confirmed to represent four samples, starting from 20, 40, 60, and 80 seconds, as shown in Figure 5(a). Each region has 8 data points (e.g., seconds 20, 22, 24, 26, 28, 30, 32, and 34). For this result, the total sample is 280. This purpose avoids errors in the training phase, comprising over and underfitting [31]. Then, the time average of these data is calculated to become a time dataset. Meanwhile, the FFT method creates a four-component frequency spectrum dataset for each region, as shown in Figure 5(b). Figure 6 shows a PCA visualization of the time dataset. The data distribution has a variance of 93.8% for PC1 and 3.8% for PC2, resulting in a total variance of 97.6%. The data distribution for frequency elements is similar to that of the time average, with a total variance of 96.9%. These values will be used as features for sensors. It can be seen that all classes are separated. However, there is a slight overlap, which needs to be more distinguished by applying machine learning.

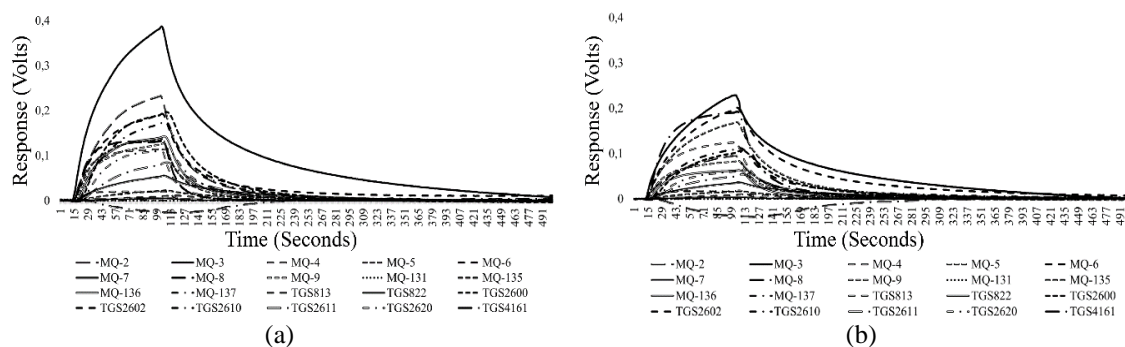


Figure 4. Gas sensor response of (a) healthy and (b) COPD subjects

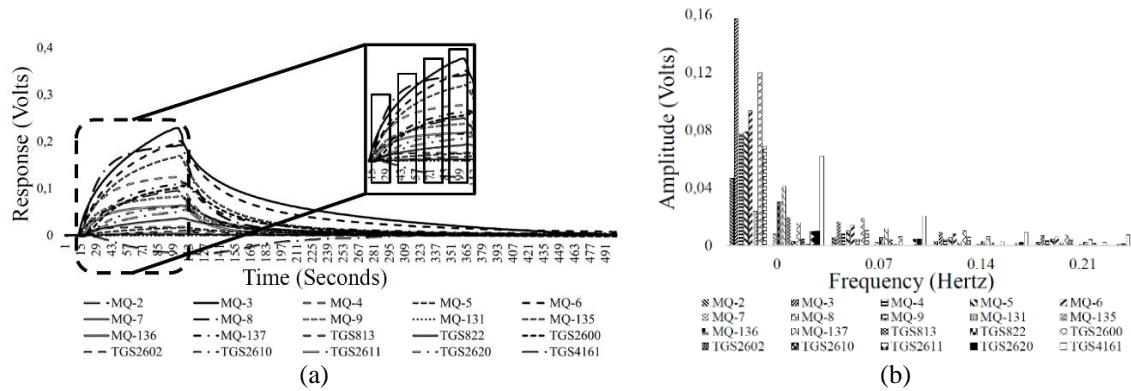


Figure 5. The gas sensor array responses of (a) time and (b) frequency elements

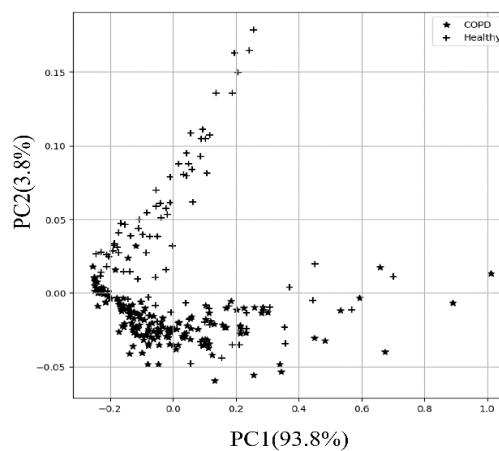


Figure 6. The data distribution of the gas sensor array visualized by PCA

3.2. Optimizing machine learning

CNN, GRU, and GCN, were optimized with their respective compositions by evaluating the entire dataset. Specifically for RF, assisted by GridSearchCV, an optimization technique from the scikit-learn library, determines acceptable parameters based on the most elevated results. This technique has three parameters: sample split, random state, and shuffle. The sample split employs stratified k-fold cross-validation, dividing the samples into the same portions, and is set at 5. The remaining parameters are set to “None” for the random state and “True” for the shuffle, making the randomization more varied to learn unseen data.

Table 4 illustrates the RF parameter optimization results according to GridSearchCV. Figure 7 shows a comparison of the classification performance of RF, ANN, CNN, GRU, and GCN. Figure 7(a) exhibits the RF performance results. For the time dataset, RF 4 achieved the highest accuracy, i.e., 81.1%. Meanwhile, for the frequency dataset, RF 6 has the highest accuracy, i.e., 79.9%. Figure 7(b) illustrates the ANN classification results for each dataset. ANN 14 gave the highest results for both time and frequency datasets of 87.1% and 87.4%, respectively. Meanwhile, ANN 15 experienced a decrease in performance, indicating this model experienced overfit. In addition, most of the ANNs provide good contributions to the frequency dataset compared to the time dataset. The performance of all CNNs can be seen in Figure 7(c). The highest CNN was achieved on the time dataset on CNN 15 with an accuracy of 86.6%. Meanwhile, on the frequency dataset, CNN 10 had an accuracy of 85.4%. However, this configuration has the lowest architecture which has implications for simple calculations. Figure 7(d) shows the performance of the cell-based memory of the GRU model. The contribution of the model is outstanding on the time dataset, with the highest accuracy of 84.9% achieved by GRU 3. Meanwhile, on the frequency dataset, all GRUs tended to have an accuracy below 70%. Figure 7(e) shows the performance of GCN variations. Compared with time dataset, GCN can differentiate between healthy and COPD subjects with high accuracy for frequency dataset. There are four GCN configurations that have an accuracy above 92%, namely GCN 5, GCN 8, GCN 9, and GCN 14. In the next stage, all these configurations will be re-evaluated with varying numbers of neurons.

Table 4. The RF parameters determined by GridSearchCV

Dataset	Model			
Time	RF 1	RF 2	RF 3	RF 4
	- Criterion = Gini	- Criterion = Gini	- Criterion = Entropy	- Criterion = Entropy
	- Max features = sqrt	- Max features = log ₂	- Max features = sqrt	- Max features = log ₂
	- Min samples leaf = 3	- Min samples leaf = 2	- Min samples leaf = 4	- Min samples leaf = 3
Frequency	RF 5	RF 6	RF 7	RF 8
	- Criterion = Gini	- Criterion = Gini	- Criterion = Entropy	- Criterion = Entropy
	- Max features = sqrt	- Max features = log ₂	- Max features = sqrt	- Max features = log ₂
	- Min samples leaf = 3	- Min samples leaf = 3	- Min samples leaf = 2	- Min samples leaf = 3
	- Min samples split = 3	- Min samples split = 6	- Min samples split = 2	- Min samples split = 5
	- Trees = 6	- Trees = 56	- Trees = 69	- Trees = 29

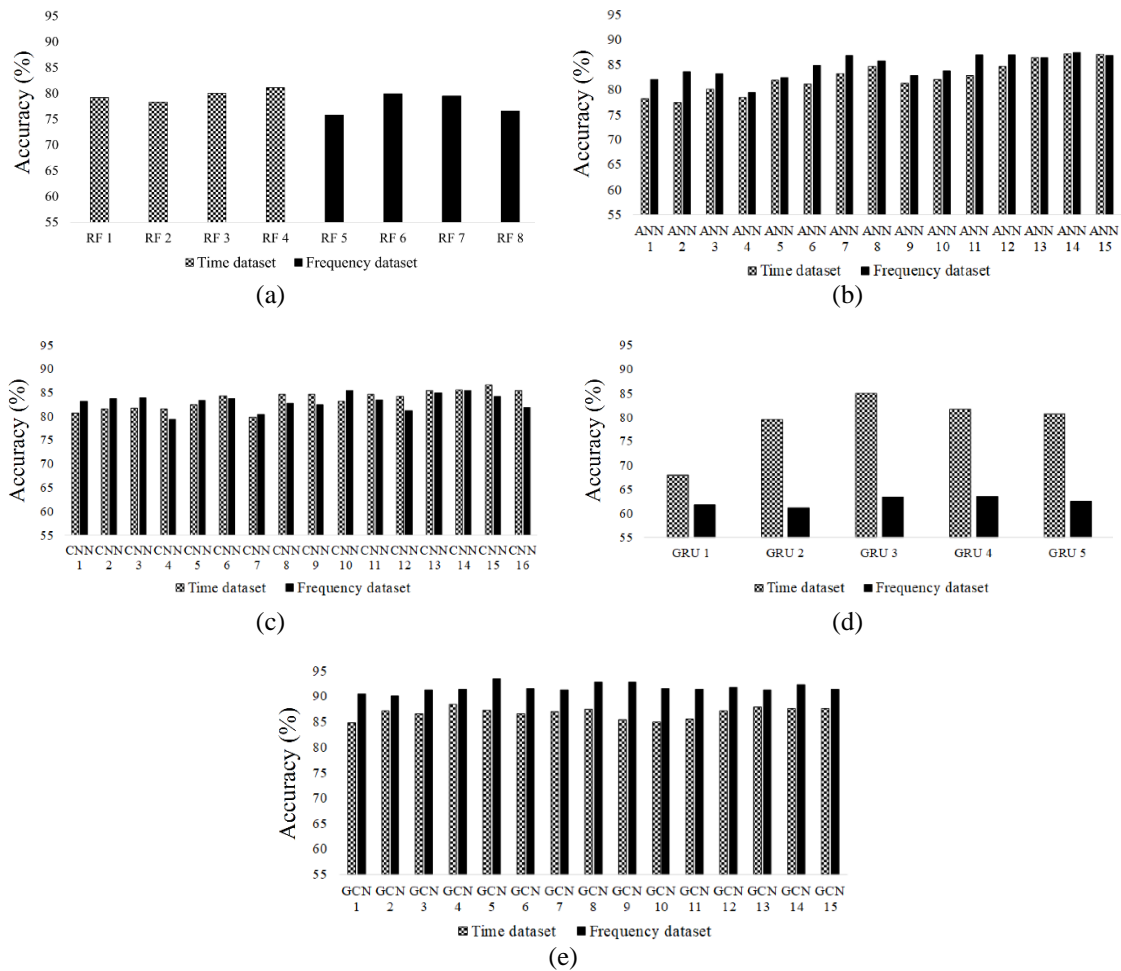


Figure 7. The classification performances of; (a) RF, (b) ANN, (c) CNN, (d) GRU, and (e) GCN

Table 5 shows a comparison of the classification performance of the modified GCN. This concludes that GCN 5 with 55 neurons provides accuracy results of 94.8%. Of all the machine learning algorithm configurations used in this experiment, GCN with a frequency spectrum dataset had the highest ability to differentiate between healthy people and COPD suspects. Figure 8 presents the performance of the electronic nose equipped with the GCN model. Figure 8(a) shows the data distribution generated by the convolution layer in the GCN with a total variance of 99.6%, which illustrates that the two classes can be separated significantly. This may fortify the reason why GCN has the highest accuracy. The selected model will be more challenging to combine with data preprocessing. Meanwhile, Figure 8(b) illustrates the loss curve during the training phase on GCN for 500 epochs. This shows that the performance of this model has a high loss value, i.e. around 10%.

Essential information extraction in PCA output can be combined with the GCN 5 configuration to be tested for its performance level. Figure 9 shows the performance of an electronic nose employing a GCN model combined with PCA data preprocessing. Figure 9(a) depicts the distribution of data produced by the convolution layer in GCN combined with PCA data preprocessing with a total variance of 99.8%, demonstrating that the two classes can be more significantly separated. Figure 9(b) illustrates the loss curve during the training phase on GCN combined with PCA for 150 epochs, which reaches an error value of 0.0053.

Table 5. The modified GCN classification performance.

Model	Neurons	Accuracy (%)
GCN 5	5	93.4
	30	93.0
	55	94.8
GCN 8	5	92.7
	30	92.2
	55	92.2
GCN 9	5	92.7
	30	90.6
	55	90.6
GCN 14	5	92.2
	30	92.6
	55	91.8

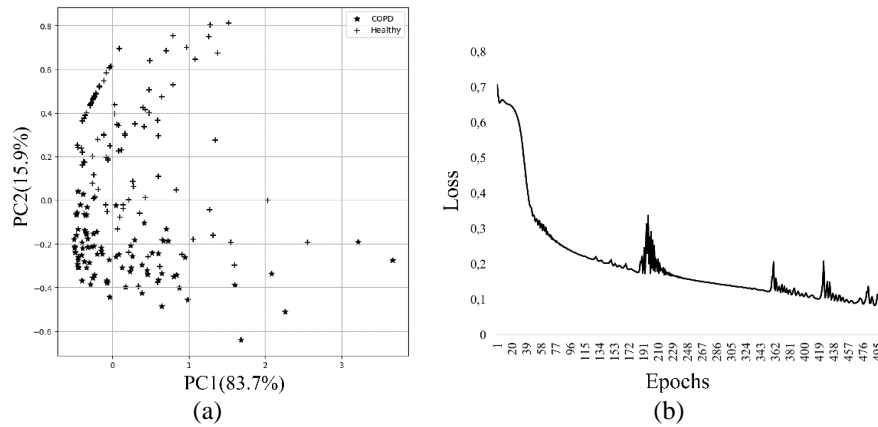


Figure 8. The GCN performance (a) the data distribution of the convolution layer and (b) the training loss curve

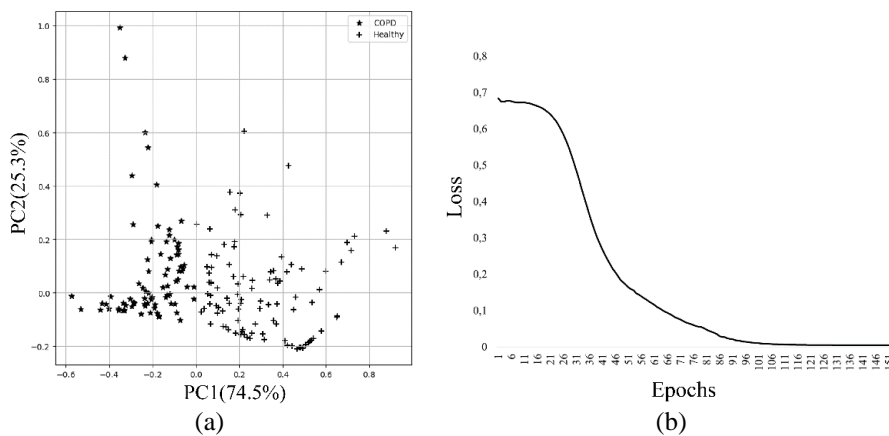


Figure 9. The performance of GCN combined with PCA data preprocessing (a) the data distribution of the convolution layer and (b) the training loss curve

This shows that combining PCA data preprocessing with GCN will accelerate achieving convergence in the training phase. Figure 10 shows the prediction of the GCN combined with PCA data preprocessing for healthy and COPD subjects. In ten tests, the combination of PCA and GCN produces an average accuracy of 97.5%, precision of 97.2%, recall of 97.4%, and F1-score of 97.5%. Therefore, this method can be used in electronic nose systems, especially those involving high-dimensional features, to improve their classification performance.

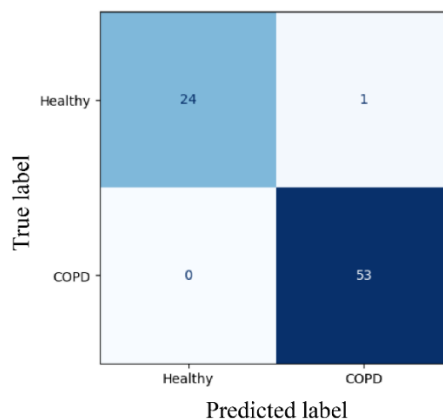


Figure 10. The prediction of the GCN combined with PCA data preprocessing for healthy and COPD subjects

4. CONCLUSION

This research developed an electronic nose method and a pattern recognition algorithm to identify COPD suspects through exhaled breath. The electronic nose consists of twenty semiconductor gas sensors. The FFT method plays a role in assessing the frequency element in the gas sensor response. Five machine learning algorithms, including RF, ANN, CNN, GRU, and GCN, were employed in this study. The GCN model that applies a frequency dataset has the highest accuracy of 94.8%. The GCN model combined with PCA data preprocessing provides a more satisfactory accuracy of 97.5%, precision of 97.2%, recall of 97.4%, and F1-score of 97.5%. Further research will develop a more portable and compact system with an optimal number of sensors and lower power consumption.

ACKNOWLEDGEMENTS

This work was funded in part by the Indonesian Ministry of Education and Culture under *Penelitian Terapan Unggulan Perguruan Tinggi (PTUPT) Program*; Asian Development Bank under Higher Education for Technology Innovation (ADB HETI) Project; and Institut Teknologi Sepuluh Nopember (ITS) under *Penelitian Dana Departemen Program and Penelitian Keilmuan Program*.




REFERENCES

- [1] A. Agustí *et al.*, "Global initiative for chronic obstructive lung disease 2023 report: GOLD executive summary," *European Respiratory Journal*, vol. 61, no. 4, Apr. 2023, doi: 10.1183/13993003.00239-2023.
- [2] H. Carrette *et al.*, "Prevalence and management of chronic breathlessness in COPD in a tertiary care center," *BMC Pulmonary Medicine*, vol. 19, no. 1, Dec. 2019, doi: 10.1186/s12890-019-0851-5.
- [3] A. J. Alfahad *et al.*, "Current views in chronic obstructive pulmonary disease pathogenesis and management," *Saudi Pharmaceutical Journal*, vol. 29, no. 12, pp. 1361–1373, Dec. 2021, doi: 10.1016/j.jsps.2021.10.008.
- [4] WHO, "Chronic obstructive pulmonary disease (COPD)," *World Health Organization*, 2023. [https://www.who.int/news-room/fact-sheets/detail/chronic-obstructive-pulmonary-disease-\(copd\)](https://www.who.int/news-room/fact-sheets/detail/chronic-obstructive-pulmonary-disease-(copd))
- [5] I. Pantazopoulos *et al.*, "Incorporating biomarkers in COPD management: the research keeps going," *Journal of Personalized Medicine*, vol. 12, no. 3, Mar. 2022, doi: 10.3390/jpm12030379.
- [6] S. Scarlata, P. Finamore, M. Meszaros, S. Dragonieri, and A. Bikov, "The role of electronic noses in phenotyping patients with chronic obstructive pulmonary disease," *Biosensors*, vol. 10, no. 11, Nov. 2020, doi: 10.3390/bios10110171.
- [7] M. Maciel, S. Sankari, M. Woollam, and M. Agarwal, "Optimization of metal oxide nanosensors and development of a feature extraction algorithm to analyze VOC profiles in exhaled breath," *IEEE Sensors Journal*, vol. 23, no. 15, pp. 16571–16578, Aug. 2023, doi: 10.1109/JSEN.2023.3288968.
- [8] H. Hendrick, R. Hidayat, G. J. Horng, and Z.-H. Wang, "Non-invasive method for tuberculosis exhaled breath classification using electronic nose," *IEEE Sensors Journal*, vol. 21, no. 9, pp. 11184–11191, May 2021, doi: 10.1109/JSEN.2021.3061616.
- [9] V. A. Binson, M. Subramoniam, Y. Sunny, and L. Mathew, "Prediction of pulmonary diseases with electronic nose using SVM and XGBoost," *IEEE Sensors Journal*, vol. 21, no. 18, pp. 20886–20895, Sep. 2021, doi: 10.1109/JSEN.2021.3100390.




- [10] D. Aulia, R. Sarno, S. C. Hidayati, and M. Rivai, "Optimization of the electronic nose sensor array for asthma detection based on genetic algorithm," *IEEE Access*, vol. 11, pp. 74924–74935, 2023, doi: 10.1109/ACCESS.2023.3291451.
- [11] M. Misbah, M. Rivai, F. Kurniawan, Z. Muchidin, and D. Aulia, "Identification of diabetes through urine using gas sensor and convolutional neural network," *International Journal of Intelligent Engineering and Systems*, vol. 15, no. 1, pp. 520–529, Feb. 2022, doi: 10.22266/ijies2022.0228.47.
- [12] H. A. Sujono, M. Rivai, and M. Amin, "Asthma identification using gas sensors and support vector machine," *TELKOMNIKA (Telecommunication Computing Electronics and Control)*, vol. 16, no. 4, pp. 1468–1480, Aug. 2018, doi: 10.12928/telkomnika.v16i4.8281.
- [13] R. Faleh, M. Othman, S. Gomri, K. Aguir, and A. Kachouri, "A transient signal extraction method of WO 3 gas sensors array to identify pollutant gases," *IEEE Sensors Journal*, vol. 16, no. 9, pp. 3123–3130, May 2016, doi: 10.1109/JSEN.2016.2521578.
- [14] N. F. Hikmah, R. Setiawan, and M. D. Gunawan, "Sleep quality assessment from robust heart and muscle fatigue estimation using supervised machine learning," *International Journal of Intelligent Engineering and Systems*, vol. 16, no. 2, pp. 319–331, Feb. 2023, doi: 10.22266/ijies2023.0430.26.
- [15] E. R. R. Sachidanandan, N. P. Singh, and S. Gunda, "Design and simulation of a low-power and high-speed fast fourier transform for medical image compression," in *HMAM2*, Mar. 2023, doi: 10.3390/HMAM2-14159.
- [16] J. Yan *et al.*, "Electronic nose feature extraction methods: a review," *Sensors*, vol. 15, no. 11, pp. 27804–27831, Nov. 2015, doi: 10.3390/s151127804.
- [17] U. A. Bhatti, H. Tang, G. Wu, S. Marjan, and A. Hussain, "Deep learning with graph convolutional networks: an overview and latest applications in computational intelligence," *International Journal of Intelligent Systems*, vol. 2023, pp. 1–28, Feb. 2023, doi: 10.1155/2023/8342104.
- [18] M. A. S. Sejan, M. H. Rahman, M. A. Aziz, J.-I. Baik, Y.-H. You, and H.-K. Song, "Graph convolutional network design for node classification accuracy improvement," *Mathematics*, vol. 11, no. 17, Aug. 2023, doi: 10.3390/math11173680.
- [19] Y. Shi, M. Liu, A. Sun, J. Liu, and H. Men, "A fast pearson graph convolutional network combined with electronic nose to identify the origin of rice," *IEEE Sensors Journal*, vol. 21, no. 19, pp. 21175–21183, Oct. 2021, doi: 10.1109/JSEN.2021.3079424.
- [20] W. Xuan, G. Jian-She, H. Bo-Jie, W. Zong-Shan, D. Hong-Wei, and W. Jie, "A lightweight modified YOLOX network using coordinate attention mechanism for PCB surface defect detection," *IEEE Sensors Journal*, vol. 22, no. 21, pp. 20910–20920, Nov. 2022, doi: 10.1109/JSEN.2022.3208580.
- [21] D. Xie, D. Chen, S. Peng, Y. Yang, L. Xu, and F. Wu, "A low power cantilever-based metal oxide semiconductor gas sensor," *IEEE Electron Device Letters*, vol. 40, no. 7, pp. 1178–1181, Jul. 2019, doi: 10.1109/LED.2019.2914271.
- [22] P. Rai and S. H. Saeed, "Detection of harmful gases present in the environment," *Indonesian Journal of Electrical Engineering and Computer Science (IJECS)*, vol. 30, no. 1, pp. 70–80, Apr. 2023, doi: 10.11591/ijeecs.v30.i1.pp70-80.
- [23] S. A. Laga and R. Sarno, "Temperature effect of electronic nose sampling for classifying mixture of beef and pork," *Indonesian Journal of Electrical Engineering and Computer Science*, vol. 19, no. 3, pp. 1626–1634, Sep. 2020, doi: 10.11591/ijeecs.v19.i3.pp1626-1634.
- [24] R. A. K. Wijaya, A. Kusumaatmaja, and D. M. Rizal, "Predicting the value of sperm analysis using an electronic nose," *Indonesian Journal of Electrical Engineering and Computer Science (IJECS)*, vol. 28, no. 1, pp. 174–182, Oct. 2022, doi: 10.11591/ijeecs.v28.i1.pp174-182.
- [25] S. Sikhakolli and A. Sikhakolli, "A bacterial foraging algorithm with random forest classifier for detecting the design patterns in source code," *International Journal of Intelligent Engineering and Systems*, vol. 14, no. 2, pp. 95–105, Apr. 2021, doi: 10.22266/ijies2021.0430.09.
- [26] P. Rai, S. H. Saeed, and S. O. Mishra, "Harmful gases detection using artificial neural networks of the environment," *Indonesian Journal of Electrical Engineering and Computer Science (IJECS)*, vol. 30, no. 3, pp. 1389–1398, Jun. 2023, doi: 10.11591/ijeecs.v30.i3.pp1389-1398.
- [27] L. Farokhah, R. Sarno, and C. Faticah, "Simplified 2D CNN architecture with channel selection for emotion recognition using EEG spectrogram," *IEEE Access*, vol. 11, pp. 46330–46343, 2023, doi: 10.1109/ACCESS.2023.3275565.
- [28] C. Manjunath, B. Marimuthu, and B. Ghosh, "Deep learning for stock market index price movement forecasting using improved technical analysis," *International Journal of Intelligent Engineering and Systems*, vol. 14, no. 5, pp. 129–141, Oct. 2021, doi: 10.22266/ijies2021.1031.13.
- [29] A. El Filali, A. Jadli, E. H. Ben Lahmer, and S. El Filali, "A novel LSTM-GRU-based hybrid approach for electrical products demand forecasting," *International Journal of Intelligent Engineering and Systems*, vol. 15, no. 3, pp. 601–613, 2022.
- [30] B. Barokah, R. Radi, L. F. Zamzami, A. Setiawan, and J. P. L. Y. Putro, "Design of sample display system on electronic nose for synthetic flavor classification," *Indonesian Journal of Electrical Engineering and Computer Science (IJECS)*, vol. 30, no. 2, pp. 690–698, May 2023, doi: 10.11591/ijeecs.v30.i2.pp690-698.
- [31] K. Alomar, H. I. Aysel, and X. Cai, "Data augmentation in classification and segmentation: a survey and new strategies," *Journal of Imaging*, vol. 9, no. 2, Feb. 2023, doi: 10.3390/jimaging9020046.

BIOGRAPHIES OF AUTHORS






Dava Aulia    is currently pursuing the master's degree with the Informatics Department, Institut Teknologi Sepuluh Nopember, Surabaya, Indonesia. His research interests include artificial intelligence, deep learning, the internet of things (IoT), embedded systems, and gas sensors. He can be contacted at email: davaaulia2000@gmail.com.






Riyanarto Sarno    received the Ph.D. degree, in 1992. He is currently a Professor with the Department of Informatics, Institut Teknologi Sepuluh Nopember (ITS). He has researched process mining for five years. He is interested in research projects on machine learning, the IoT, knowledge engineering, enterprise computing, and information management. He is the author of more than five books and over 300 scientific articles, making him the world top 2% scientist in 2020 by Standford University. He can be contacted at email: riyanarto@if.its.ac.id.






Shintami Chusnul Hidayati    received the B.S. degree in informatics from Institut Teknologi Sepuluh Nopember (ITS), Surabaya, Indonesia, and the M.S. and Ph.D. degrees in computer science and information engineering from the National Taiwan University of Science and Technology, Taipei, Taiwan. She is currently a Lecturer with the Department of Informatics, ITS. Before joining ITS, she was a Postdoctoral Research Associate with the Research Center for Information Technology Innovation, Academia Sinica, Taipei, from 2017 to 2019. Her current research interests include machine learning and data mining and their applications to multimedia analysis, information retrieval, and computer vision. She can be contacted at email: shintami@its.ac.id.



Alfian Nur Rosyid    is a lecturer, researcher, and respiratory specialist actively involved in education, research, and healthcare at the Faculty of Medicine, Airlangga University, and Airlangga University Hospital. He has been serving as a staff member in the Department of Pulmonology and Respiratory Medicine at the Faculty of Medicine, Airlangga University, since 2015. Various research projects led by him have been published in various national and international journals. His research encompasses topics such as asthma, COPD, lung infections, including COVID-19, and others. He has received several awards, including first place in an oral presentation competition organized by the Indonesian Society of Respirologists. He has authored numerous books, including those on tuberculosis, HIV, and medical emergencies. He can be contacted at email: alfian-n-r-10@fk.unair.ac.id.



Muhammad Rivai    received the Ph.D. degree, in 2006. He is currently a Lecturer with the Department of Electrical Engineering, Institut Teknologi Sepuluh Nopember, Surabaya, Indonesia. His research interests include sensors, chemical sensors, gas sensors, electronics, robotics, and artificial intelligence applications. He can be contacted at email: muhammad_rivai@ee.its.ac.id.